Fast long-wavelength exchange spin waves in partially compensated Ga:YIG

T. Böttcher; M. Ruhwedel; K. O. Levchenko; Q. Wang ⓘ ; H. L. Chumak; M. A. Popov ⓘ ; I. V. Zavislyak; C. Dubs ⓘ ; O. Surzhenko ⓘ ; B. Hillebrands; A. V. Chumak ⓘ ; P. Pirro ✉ ⓘ

Check for updates
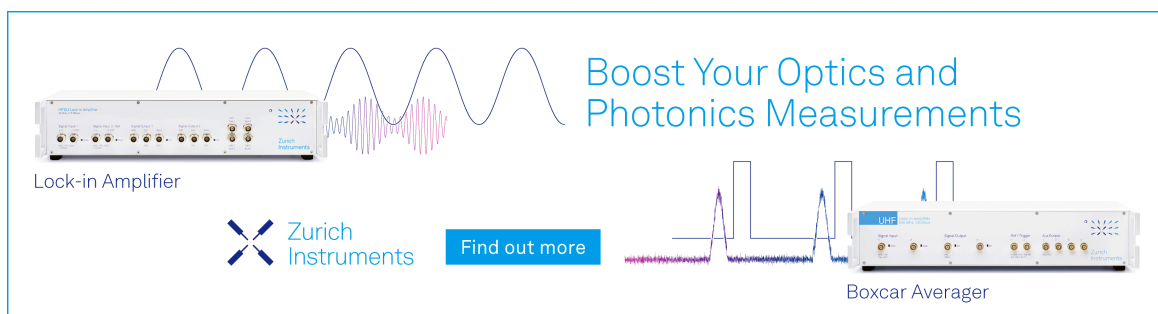
View Online   Export Citation

29 April 2024 08:00:21

Fast long-wavelength exchange spin waves in partially compensated Ga:YIG

T. Böttcher,[1,2] M. Ruhwedel,[1] K. O. Levchenko,[3] Q. Wang,[3] (iD) H. L. Chumak,[4] M. A. Popov,[4] (iD) I. V. Zavislyak,[4] C. Dubs,[5] (iD) O. Surzhenko,[5] (iD) B. Hillebrands,[1] A. V. Chumak,[3] (iD) and P. Pirro[1,a] (iD)

AFFILIATIONS

[1]Fachbereich Physik and Landesforschungszentrum OPTIMAS, Technische Universität Kaiserslautern,
 Gottlieb-Daimler-Straße 46, 67663 Kaiserslautern, Germany
[2]MAINZ Graduate School of Excellence, Staudingerweg 9, 55128 Mainz, Germany
[3]Faculty of Physics, University of Vienna, Boltzmanngasse 5, A-1090 Wien, Austria
[4]Faculty of Radiophysics, Electronics and Computer Systems, Taras Shevchenko National University of Kyiv, Kyiv 01601, Ukraine
[5]INNOVENT e.V. Technologieentwicklung, Prüssingstrasse 27B, 07745 Jena, Germany

[a]Author to whom correspondence should be addressed: ppirro@physik.uni-kl.de

ABSTRACT

Spin waves in yttrium iron garnet (YIG) nano-structures attract increasing attention from the perspective of novel magnon-based data proc-essing applications. For short wavelengths needed in small-scale devices, the group velocity is directly proportional to the spin-wave exchange stiffness constant λ_{ex}. Using wave vector resolved Brillouin light scattering spectroscopy, we directly measure λ_{ex} in Ga-substituted YIG thin films and show that it is about three times larger than for pure YIG. Consequently, the spin-wave group velocity overcomes the one in pure YIG for wavenumbers $k > 4 \, \text{rad}/\mu\text{m}$, and the ratio between the velocities reaches a constant value of around 3.4 for all $k > 20 \, \text{rad}/\mu\text{m}$. As revealed by vibrating-sample magnetometry and ferromagnetic resonance spectroscopy, Ga:YIG films with thicknesses down to 59 nm have a low Gilbert damping ($\alpha < 10^{-3}$), a decreased saturation magnetization $\mu_0 M_S \approx 20$ mT, and a pronounced out-of-plane uniaxial anisotropy of about $\mu_0 H_{u1} \approx 95$ mT, which leads to an out-of-plane easy axis. Thus, Ga:YIG opens access to fast and isotropic spin-wave transport for all wavelengths in nano-scale systems independently of dipolar effects.

Wave-based logic concepts[1–3] are expected to come along with major advantages over information processing based on current CMOS-based information technology.[4,5] In particular, coherent spin waves[6] are envisaged to allow for the realization of efficient wave-based logic devi-ces.[3,7–12] However, progress in this field places high demands on the materials used. Specifically, spin-wave elements operating at large clock frequencies demand materials that exhibit a small Gilbert damping con-stant,[13] large spin-wave velocities, and good processing properties. Yttrium iron garnet (YIG) has a very small damping constant,[14] and nano-structures of 50 nm lateral sizes have been demonstrated recently.[15–17] However, dipolar spin waves in YIG waveguides feature velocities that are significantly reduced compared to plane YIG films,[16] which are caused by the flattening of the dispersion curve. The fastest dipolar waves in these structures are magnetostatic surface waves, which offer a group velocity of around 0.2 μm/ns.[17] Exchange spin waves with wavelengths in the range of 100 nm or shorter are faster,[18] but the

excitation of such short wavelengths is a separate challenge.[16] It can be addressed by the utilization of nanoscopic antennas with increased Ohmic loss, strongly non-uniform magnetic patterns,[19] hybrid nano-structures utilizing different magnetic materials,[20–22] or more complex physical phenomena like magnon Cherenkov radiation.[23]

To operate with waves of maximized speed in nano-structures, materials with large spin-wave exchange stiffness $\lambda_{ex} = 2A/(\mu_0 M_S)$ are mandatory since the exchange contribution to the group velocity is directly proportional to λ_{ex}. Here, A is the Heisenberg exchange con-stant, M_S is the saturation magnetization, and μ_0 is the permeability of the vacuum. In addition, the possibility to operate with fast exchange-dominated spin waves of larger wavelengths would not only allow for the operations with "standard" micro-scaled antennas,[11,16] but also would give the freedom required for engineering of data-processing units[1,24] since the exchange-dominated dispersion relation is highly isotropic.

In this context, it is promising to study ferrimagnetic insulators that are close to the magnetic compensation since low M_S tends to increase λ_{ex}. For this, liquid phase epitaxy (LPE) based[14] growth of Ga-substituted YIG,[25–29] which has been adopted for deposition of $Y_3Fe_{5-x}Ga_xO_{12}$ single crystalline films of sub-100 nm thicknesses, is very interesting. In these films, non-magnetic Ga^{3+} ions preferentially substitute the magnetic Fe^{3+} ions in the tetrahedral coordinated magnetic sub-lattice ($0 < x < 1.5$), decreasing the M_S of this ferrimagnetic material down to the fully compensated antiferromagnetic state (for single crystals grown from high-temperature solutions at contents x of about 1.27 formula units at room temperature $T = 295K$).[25,26] Aside from that Ga substitution induces a strong out-of-plane uniaxial anisotropy, enabling the easy axis of the thin film perpendicular to the film surface.

Here, we report on the investigation of the spin waves in Ga:YIG films of sub-100 nm thickness. Ga substitution $x \approx 1$ was chosen so that the magnetization of the sample is decreased to one tenth of the pure YIG value. This was done in order to change the easy magnetization orientation from the in-plane to out-of-plane, simultaneously avoiding an excessive increase in the magnetic damping. First, a thorough characterization is performed using ferromagnetic resonance spectroscopy (FMR) in combination with vibrating-sample magnetometry (VSM) to obtain saturation magnetization, anisotropy constants, and damping parameters. Afterwards, wave vector resolved[29,30] Brillouin light scattering (BLS) spectroscopy is used to measure the dispersion relation of thermal spin waves $\omega(k)$ and the spin-wave exchange stiffness λ_{ex} directly. The resulting group velocity $d\omega/dk$ is compared to the velocities of spin waves in pure YIG films. Our presented results are complementary and in good agreement with recent results from an indirect measurement of the dispersion relation at low wave vectors using electrical spectroscopy in Ga:YIG reported by Carmiggelt et al.[31]

In the following, we present exemplary broadband ferromagnetic resonance-vector network analyzer (FMR-VNA) spectroscopy data for a LPE-grown 59 nm thick film of Ga:YIG/GGG(111). Data for the other films' thicknesses of 105 nm-thick Ga:YIG/GGG(111), 95 nm-thick Ga:YIG/GGG(001), and a reference film of 97 nm-thick YIG/GGG(111) are provided in the supplementary material. The films grown on GGG(111) were cut into square specimens with the edges oriented along [11$\bar{2}$] and [1$\bar{1}$0] crystallographic directions and samples on GGG (001)—along [100] and [010] (see Figs. S1 and S5 in the supplementary material). For magnetic characterization, FMR-VNA was performed in the frequency range up to 20 GHz and at the rf power of 0 dBm. To define the crystallographic parameters of the samples, the theoretical model of Bobkov and Zavislyak was used.[32] The model differentiates three main anisotropy fields—a cubic field H_c, a uniaxial anisotropy field of the first order H_{u1}, and a uniaxial anisotropy field of the second order H_{u2}. The cubic anisotropy originates from the magnetization along the preferred crystallographic directions in the garnet lattice,[14,32] while the uniaxial anisotropy consists of cubic, growth-induced, and strain-induced contributions resulting in an effective uniaxial anisotropy.[14,33,34] In addition to the direction of a magnetic field H, the FMR frequency also depends on the crystallographic orientation of the GGG substrate.[32] To define all the

anisotropy fields experimentally, a magnetic field was applied in-plane (IP) along the two orthogonal crystallographic axes [11$\bar{2}$] and [1$\bar{1}$0] (corresponding to the sample's edges) and out-of-plane (OOP) along the [111] direction normal to the film plane. The saturation magnetization M_s was measured by VSM. Detailed descriptions of the employed theoretical model, the measurement procedure, and the FMR analyses for the film under investigation are given in the supplementary material.

The dependence of the FMR frequency on the in-plane magnetic field is shown in Fig. 1(a). The Gilbert damping parameter α and the inhomogeneous linewidth broadening $\Delta H(0)$ were found according to the standard approach described in Ref. 35 [see Fig. 1(b)], taking into consideration that $H_{u1} > M_s$. All obtained parameters are summarized in Fig. 1(c) along with the results of a reference 97 nm-thick YIG/GGG(111) film. A comparison of these values demonstrates that Ga doping led to a $\simeq$ 9 times reduction in the saturation magnetization M_s, a $\simeq$ 27 times increase in the uniaxial anisotropy H_{u1}, and a $\simeq$ 4.7 times increase in the Gilbert damping α. A strong increase in the uniaxial anisotropy indicates the out-of-plane easy axis of a Ga:YIG thin film. While an increase in α was observed, it is still significantly lower compared to metallic compounds[2] and better[36] or comparable[37] to other doped YIG films, e.g., using bismuth-doping.[37,38] A detailed comparison of the material parameters of our Ga:YIG with those alternative materials including Bi:YIG is given in the supplementary material. The obtained values for Ga:YIG are also in good agreement with those reported in Ref. 31.

After the characterization via FMR, the dispersion relation of thermally excited, magnetostatic surface spin waves propagating perpendicularly to the applied field is probed by BLS spectroscopy[30] to obtain the exchange stiffness λ_{ex}. An external field of $\mu_0 H = 300\,\text{mT}$ is applied in the film plane along the sample edge, which ensures an in-plane magnetization. For the spectral analysis of the scattered light, a six-pass tandem Fabry–Pérot interferometer is used.[39] In all measurements presented here, a laser with a wavelength of $\lambda_{Laser} = 491\,\text{nm}$ is used. The in-plane component k_ζ of the wave vector of the probed spin wave is varied by changing the angle of light incidence Θ, $k_\zeta = 4\pi \sin(\Theta)/\lambda_{Laser}$—see Fig. 2(a). The results for the 59 nm thick Ga:YIG film are presented in Fig. 2. Figure 2(b) shows three exemplary BLS spectra (anti-stokes part). Data for three different in-plane wave vectors are presented. Aside from the quite strong phonon signal, one can distinguish the fundamental spin-wave mode and the first perpendicular standing spin-wave mode (PSSW). For wave vectors between 12 and 20 rad μm^{-1}, no fundamental mode could be observed because of the strong signal of the phonon mode that crosses the fundamental spin-wave mode in this area (see, e.g., the spectrum for $k_\zeta = 14.7\,\text{rad}\,\mu m^{-1}$).

The corresponding analytical description of the spin-wave dispersion relation for the case of a ferromagnetic film in the (111) orientation having uniaxial and cubic anisotropy with unpinned surface spins has been obtained by Kalinikos et al.[40] The wave vector quantization along the film normal, which results in the appearance of the PSSWs,[41] is described by the index n such that the dispersion relation is given by

$$f_n(\mathbf{k}) = \frac{\gamma \mu_0}{2\pi} \sqrt{\left(H + \lambda_{ex}k_n^2 + M_S - M_S P_{nn}(k_\zeta t) - H_c - H_{u1}\right)\left(H + \lambda_{ex}k_n^2 + M_S P_{nn}(k_\zeta t)\sin^2\phi\right) - 2H_c^2\cos^2 3\phi_M},\quad (1)$$
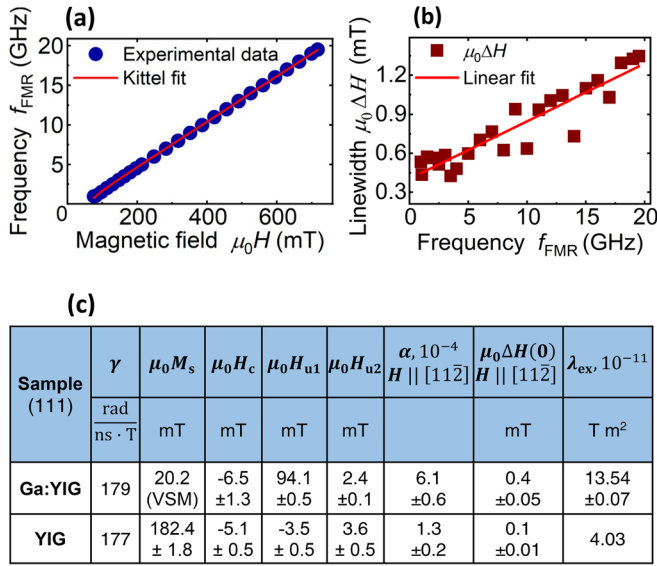
FIG. 1. (a) Ferromagnetic resonance frequency f_{FMR} as a function of the in-plane magnetic field $H||[11\bar{2}]$. Experimental data (blue dots) are fitted by a modified Kittel equation (solid red line). (b) Recalculated full width at half maximum (FWHM) field linewidth $\mu_0\Delta H$ as a function of f_{FMR}. Measured data (dark red squares) are fitted by a linear regression (solid red line). A full evaluation (see the supplementary material) provides the values shown in table (c). (c) Parameters obtained from FMR-VNA data of 59 nm Ga:YIG and 97 nm YIG films grown on GGG(111).

where $k_n = \sqrt{k_\zeta^2 + \kappa_n^2}$ is the total spin wave vector consisting of the in-plane spin wave vector k_ζ and the out-of-plane spin wave vector κ_n with $\kappa_n = n\pi/t$, $n = 0, 1, 2, \ldots$. Here, t is the thickness of the film, ϕ is the angle between the static magnetization and the in-plane wave vector k_ζ, ϕ_M is the angle between the static magnetization and the $[1\bar{1}0]$ axis, H is the applied magnetic field, and γ is the gyromagnetic ratio that we take from the FMR measurements. The matrix element P_{nn} is a function of $k_\zeta t$ ($0 \le P_{nn} < 1$ if $0 \le k_\zeta t < \infty$). In the long

wavelength limit ($k_\zeta t \ll 1$) and for unpinned surface spins, the following approximations have been obtained: $P_{00} = k_\zeta t/2$ for $n = 0$ and $(k_\zeta t/n\pi)^2$ for $n \neq 0$.[42]

The dispersion relations of the respective modes extracted from the BLS spectra are shown in Fig. 2(c) together with fit curves according to Eq. (1). FMR measurements show that H_c is about one order of magnitude smaller than H_{u1} [compare Fig. 1(c)]. Consequently, the last term in Eq. (1) that is quadratic in H_c can be safely neglected. For the fits, we have fixed the saturation magnetization to $\mu_0 M_S = 20.2$ mT as obtained from VSM and the gyromagnetic ratio to $\gamma = 179$ rad $T^{-1}ns^{-1}$ as obtained from the FMR measurements. The extracted values from the simultaneous fits of the fundamental mode and the first PSSW mode are exchange stiffness $\lambda_{ex} = (13.54 \pm 0.07) \times 10^{-11}$ Tm^2 and exchange constant $A = (1.37 \pm 0.01)$ pJm^{-1}, respectively. The sum of the anisotropy fields is $\mu_0(H_u + H_c) = (91.3 \pm 0.4)$ mT, in very good agreement with the values obtained from FMR [compare to Fig. 1(c)].

The exchange stiffness in the film under investigation in this work is about three times as large as the one for pure YIG.[43] This results in a much higher group velocity than in pure YIG as can be seen in Fig. 3. There the fitted dispersion relation of the fundamental mode for the investigated Ga:YIG film and the corresponding dispersion relation for a pure YIG film of the same thickness of 59 nm and at the same applied field of 300 mT is also shown. Here, the standard parameters of YIG[14,43] have been used: $\gamma = 177$ rad $T^{-1}ns^{-1}$ (from FMR), $\lambda_{ex} = 4.03 \times 10^{-11}$ Tm^2, and $\mu_0 M_S = 177.2$ mT. (All anisotropy contributions are neglected.) The corresponding group velocities calculated by $v_{gr} = 2\pi \partial f_n(\mathbf{k})/\partial k_n$ are plotted in the lower part of Fig. 3(b). The exchange dominated region is characterized by a linear dependence of the group velocity on the wave vector. Thus, spin waves in Ga:YIG can be considered as exchange dominated down to very low wave vectors as it is directly visible from Fig. 3(b). For wave vectors above $k_\zeta > 4$ rad μm^{-1}, spin-waves in Ga:YIG are faster compared to pure YIG. For wave vectors $k_\zeta > 30$ rad μm^{-1}, both dispersion relations are exchange dominated, and the ratio r of the group velocities is converging to the ratio of the exchange stiffness constants $r \approx \lambda_{ex}(\text{Ga:YIG})/\lambda_{ex}(\text{YIG}) \approx 3.4$. Please note that this comparison of group velocities strongly depends on the chosen geometry;
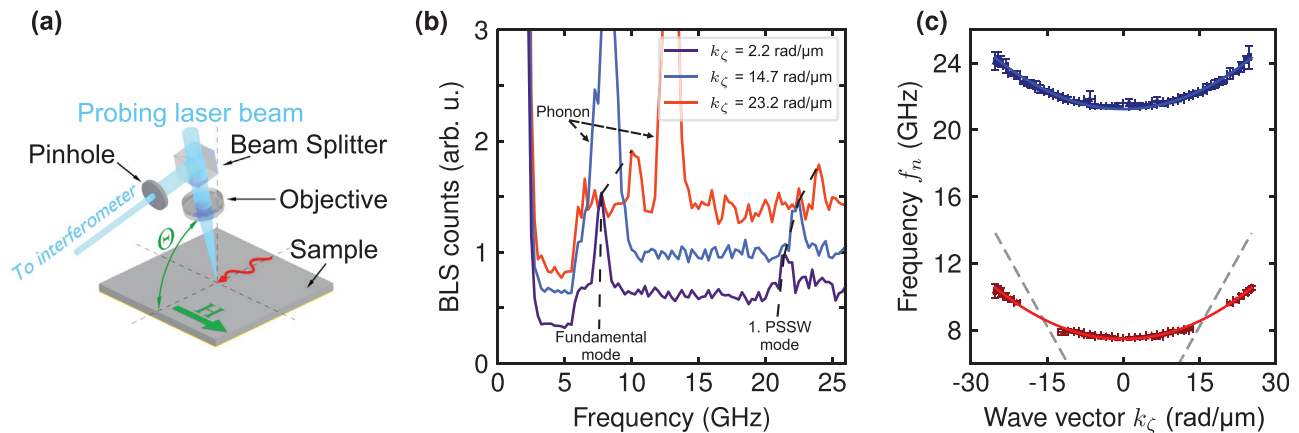

FIG. 2. (a) Schematic BLS setup. (b) Three exemplary BLS spectra obtained for different in-plane wave vectors from a 59 nm thick Ga:YIG film at an applied field of 300 mT. Two spin-wave modes as well as a phonon mode can be observed. (c) Dispersion relations for the spin-wave modes extracted from all the measured BLS spectra. The solid lines are fits according to the model given in Eq. (1). The dashed lines are linear fits of the phonon mode.
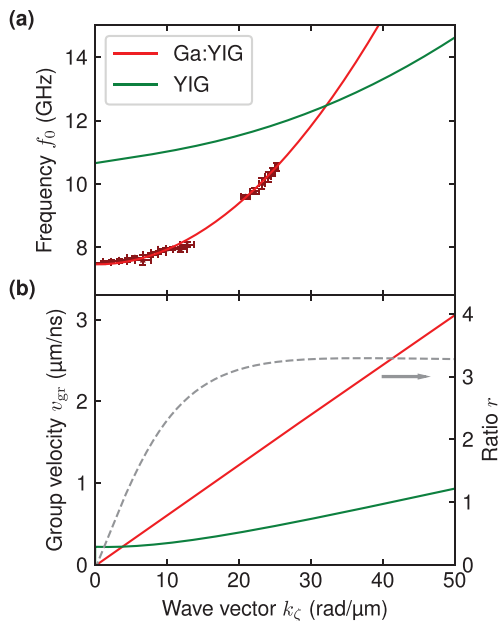
FIG. 3. (a) Dispersion fitted to the measured data from the investigated 59 nm thick Ga:YIG film at an applied field of 300 mT according to Eq. (1) (red) and a theoretical dispersion calculated according to Eq. (1) for a pure YIG film (green) of the same thickness at the same applied field using standard YIG parameters (see the text). (b) Group velocity calculated from the dispersion relation in (a) for Ga:YIG (red) and pure YIG (green). The ratio r of the group velocities for Ga:YIG and pure YIG is plotted by a gray dashed line.

for propagation along the static magnetization ($\phi = 0$), the dipolar dominated waves in YIG are even slower. As a result, for $\phi = \pi/2$, the exponential amplitude decay length $\delta = v_{gr} \cdot \tau$ (where τ is the lifetime of the magnon, calculated based on the value of α and neglected an potential influence of the inhomogeneous broadening ΔH_0[16]) might be still larger for pure YIG ($\delta \approx 40~\mu m$, for a wave vector of $k_\zeta = 15~\text{rad}~\mu m^{-1}$) compared to Ga:YIG ($\delta \approx 35~\mu m$ for the same k_ζ). However, for propagation with the same wave vector along the static magnetization ($\phi = 0$), the YIG decay length drops drastically (below $10~\mu m$) due to the changed dipolar contribution, whereas Ga:YIG preserves its large $\delta \approx 35~\mu m$ due to its isotropic, exchange-dominated group velocity. In addition, Ga:YIG is expected to maintain its decay length also for lower film thicknesses, whereas the decay length in YIG can significantly drop due to changed dipolar contribution.

Please note also that the challenge to achieve the perpendicular magnetic anisotropy while preserving the low magnetic losses was explored in other YIG-based materials[36–38] by using substrates with enlarged lattice parameters to achieve strong tensile stress. However, this approach might fail at larger film thicknesses[38] and has no significant influence on the saturation magnetization. Therefore, the exchange stiffness is not significantly increased in those systems leading to much slower spin-waves in the exchange dominated regime compared to Ga:YIG.

In conclusion, we have investigated spin-wave properties in Ga-substituted YIG with significantly decreased saturation magnetization $\mu_0 M_S \approx 20$ mT and increased exchange stiffness $\lambda_{ex} = (13.54 \pm 0.07) \times 10^{-11}$ T m^2. The saturation magnetization M_S was measured using VSM, the three anisotropy constants H_c, H_{u1}, and H_{u2} and the gyromagnetic ratio γ were determined using FMR, and the exchange stiffness λ_{ex} was determined from BLS measurements of the dispersion relation of the fundamental and the first PSSW mode. We find that even spin waves of relatively small wave vector $k \approx 4~\text{rad}/\mu m$ exhibit the exchange nature, and their velocities are higher than in pure YIG, reaching a ratio of approximately 3.4 as defined by the ratio of the individual exchange stiffness constants. As a further consequence, waves in Ga:YIG have a significantly more isotropic dispersion relation than waves of the same wavelength in YIG. Thus, for magnonic waveguides structured from Ga:YIG, only a weak dependence of important parameters, such as the wave velocity and the wave phase accumulation, on the structure sizes and on the magnetization orientation can be expected. The small saturation magnetization and the uniaxial anisotropy lead to an out-of-plane easy axis, which also facilitates the use of the entirely isotropic forward volume waves. Since the relative drop of the exchange constant A with Ga substitution x is weaker than the drop of the saturation magnetization M_s, one can expect that a further reduction of M_s by increased Ga substitution will lead to even faster and more isotropic spin waves. Eventually, a fully compensated Ga:YIG film might serve as a model system for antiferromagnetic magnonics. Thus, Ga:YIG opens access to the operation with fast and isotropic exchange spin waves of variable wavelengths in future magnonics networks.

See the supplementary material for the detailed description of the FMR measurements and of the used model to analyze the FMR data for different directions of the applied bias field. Also, an overview of the measured parameters for other Ga:YIG film thicknesses and substrate orientations is provided. In addition, a comprehensive comparison of the material parameters obtained in this work to other substituted YIG thin films is presented.

AUTHOR DECLARATIONS

Conflict of Interest

The authors declare no competing interests.

DATA AVAILABILITY

The data that support the findings of this study are available from the corresponding author upon reasonable request.

REFERENCES

[1]A. Mahmoud, F. Ciubotaru, F. Vanderveken, A. V. Chumak, S. Hamdioui, C. Adelmann, and S. Cotofana, J. Appl. Phys. **128**, 161101 (2020).

29 April 2024 08:00:21

[2]A. Barman, G. Gubbiotti, S. Ladak, A. O. Adeyeye, M. Krawczyk, J. Gräfe, C. Adelmann, S. Cotofana, A. Naeemi, V. I. Vasyuchka, B. Hillebrands *et al.*, J. Phys.: Condens. Matter **33**, 413001 (2021).

[3]A. V. Chumak, P. Kabos, M. Wu, C. Abert, C. Adelmann, A. Adeyeye, J. Åkerman, F. G. Aliev, A. Anane, A. Awad, C. H. Back *et al.*, arXiv:2111.00365 (2021).

[4]M. M. Waldrop, Nature **530**, 144 (2016).

[5]B. Dieny, I. L. Prejbeanu, K. Garello, P. Gambardella, P. Freitas, R. Lehndorff, W. Raberg, U. Ebels, S. O. Demokritov, J. Akerman *et al.*, Nat. Electron. **3**, 446 (2020).

[6]P. Pirro, V. Vasyuchka, A. A. Serga, and B. Hillebrands, Nat. Rev. Mater. **6**, 1114 (2021).

[7]A. Khitun, M. Bao, and K. L. Wang, J. Phys. D: Appl. Phys. **43**, 264005 (2010).

[8]A. V. Chumak, A. A. Serga, and B. Hillebrands, Nat. Commun. **5**, 4700 (2014).

[9]T. Fischer, M. Kewenig, D. A. Bozhko, A. A. Serga, I. I. Syvorotka, F. Ciubotaru, C. Adelmann, B. Hillebrands, and A. V. Chumak, Appl. Phys. Lett. **110**, 152401 (2017).

[10]G. Talmelli, T. Devolder, N. Träger, J. Förster, S. Wintz, M. Weigand, H. Stoll, M. Heyns, G. Schütz, I. P. Radu *et al.*, Sci. Adv. **6**, eabb4042 (2020).

[11]Q. Wang, M. Kewenig, M. Schneider, R. Verba, F. Kohl, B. Heinz, M. Geilen, M. Mohseni, B. Lägel, F. Ciubotaru *et al.*, Nat. Electron. **3**, 765 (2020).

[12]A. N. Mahmoud, F. Vanderveken, C. Adelmann, F. Ciubotaru, S. Hamdioui, and S. Cotofana, IEEE Trans. Magn. **57**, 1 (2021).

[13]T. L. Gilbert, IEEE Trans. Magn. **40**, 3443 (2004).

[14]C. Dubs, O. Surzhenko, R. Thomas, J. Osten, T. Schneider, K. Lenz, J. Grenzer, R. Hübner, and E. Wendler, Phys. Rev. Mater. **4**, 024416 (2020).

[15]Q. Wang, B. Heinz, R. Verba, M. Kewenig, P. Pirro, M. Schneider, T. Meyer, B. Lägel, C. Dubs, T. Brächer, and A. V. Chumak, Phys. Rev. Lett. **122**, 247202 (2019).

[16]B. Heinz, T. Brächer, M. Schneider, Q. Wang, B. Lägel, A. M. Friedel, D. Breitbach, S. Steinert, T. Meyer, M. Kewenig, C. Dubs, P. Pirro, and A. V. Chumak, Nano Lett. **20**, 4220 (2020).

[17]B. Heinz, Q. Wang, M. Schneider, E. Weiß, A. Lentfert, B. Lägel, T. Brächer, C. Dubs, O. V. Dobrovolskiy, P. Pirro, and A. V. Chumak, Appl. Phys. Lett. **118**, 132406 (2021).

[18]A. V. Chumak, in *Spintronics Handbook: Spin Transport and Magnetism*, 2nd ed. (CRC Press, 2019), pp. 247–302.

[19]S. Wintz, V. Tiberkevich, M. Weigand, J. Raabe, J. Lindner, A. Erbe, A. Slavin, and J. Fassbender, Nat. Nanotechnol. **11**, 948 (2016).

[20]H. Yu, Od. Kelly, V. Cros, R. Bernard, P. Bortolotti, A. Anane, F. Brandl, F. Heimbach, and D. Grundler, Nat. Commun. **7**, 11255 (2016).

[21]P. Che, K. Baumgaertl, A. Kúkol'ová, C. Dubs, and D. Grundler, Nat. Commun. **11**, 1445 (2020).

[22]C. Liu, J. Chen, T. Liu, F. Heimbach, H. Yu, Y. Xiao, J. Hu, M. Liu, H. Chang, T. Stueckler *et al.*, Nat. Commun. **9**, 738 (2018).

[23]O. Dobrovolskiy, Q. Wang, D. Y. Vodolazov, B. Budinska, R. Sachser, A. Chumak, M. Huth, and A. Buzdin, arXiv:2103.10156 (2021).

[24]U. Garlando, Q. Wang, O. Dobrovolskiy, A. Chumak, and F. Riente, arXiv:2109.12973 (2021).

[25]P. Hansen, P. Röschmann, and W. Tolksdorf, J. Appl. Phys. **45**, 2728 (1974).

[26]P. Görnert and C. d'Ambly, Phys. Status Solidi A **29**, 95 (1975).

[27]J. Guigay, J. Baruchel, D. Challeton, J. Daval, and F. Mezei, J. Magn. Magn. Mater. **51**, 342 (1985).

[28]P. Röschmann, IEEE Trans. Magn. **17**, 2973 (1981).

[29]J. W. Boyle, J. G. Booth, A. D. Boardman, I. Zavislyak, V. Bobkov, and V. Romanyuk, J. Phys. IV **7**, C1-497 (1997).

[30]T. Sebastian, K. Schultheiss, B. Obry, B. Hillebrands, and H. Schultheiss, Front. Phys. **3**, 1589 (2015).

[31]J. J. Carmiggelt, O. C. Dreijer, C. Dubs, O. Surzhenko, and T. van der Sar, Appl. Phys. Lett. **119**, 202403 (2021).

[32]V. Bobkov and I. Zavislyak, Phys. Status Solidi A **164**, 791 (1997).

[33]I. Zavislyak and M. Popov, *Yttrium: Compounds, Production and Applications*, edited by B. D. Volkerts (Nova Science Publishers, Incorporated, 2011), pp. 87–126.

[34]P. Röschmann and W. Tolksdorf, Mater. Res. Bull. **18**, 449 (1983).

[35]S. S. Kalarickal, P. Krivosik, M. Wu, C. E. Patton, M. L. Schneider, P. Kabos, T. J. Silva, and J. P. Nibarger, J. Appl. Phys. **99**, 093909 (2006).

[36]J. Chen, C. Wang, C. Liu, S. Tu, L. Bi, and H. Yu, Appl. Phys. Lett. **114**, 212401 (2019).

[37]L. Soumah, N. Beaulieu, L. Qassym, C. Carrétéro, E. Jacquet, R. Lebourgeois, J. Ben Youssef, P. Bortolotti, V. Cros, and A. Anane, Nat. Commun. **9**(1), 3355 (2018).

[38]Y. Lin, L. Jin, H. Zhang, Z. Zhong, Q. Yang, Y. Rao, and M. Li, J. Magn. Magn. Mater. **496**, 165886 (2020).

[39]B. Hillebrands, Rev. Sci. Instrum. **70**, 1589 (1999).

[40]B. A. Kalinikos, M. P. Kostylev, N. V. Kozhus, and A. N. Slavin, J. Phys.: Condens. Matter **2**, 9861 (1990).

[41]M. H. Seavey and P. E. Tannenwald, Phys. Rev. Lett. **1**, 168 (1958).

[42]B. A. Kalinikos and A. N. Slavin, J. Phys. C: Solid State Phys. **19**, 7013 (1986).

[43]S. Klingler, A. V. Chumak, T. Mewes, B. Khodadadi, C. Mewes, C. Dubs, O. Surzhenko, B. Hillebrands, and A. Conca, J. Phys. D: Appl. Phys. **48**, 015001 (2015).

29 April 2024 08:00:21